Deep-learning based automatic segmentation of vesicles in cryo-electron tomograms

This manuscript (permalink) was automatically generated from aseedb/deep-prepyto-paper@9c916f8 on September 8, 2022.

Authors

- **Amin Khosrozadeh***
  XXXX-XXXX-XXXX-XXXX · ameen-khosrowzadeh
  Institute of Anatomy, University of Bern, Bern, Switzerland; Graduate School for Cellular and Biomedical Sciences, University of Bern · Funded by Grant XXXXXXXX

- **Raphaela Seeger***
  XXXX-XXXX-XXXX-XXXX · elatella
  Institute of Anatomy, University of Bern, Bern, Switzerland; Graduate School for Cellular and Biomedical Sciences, University of Bern

- **Julika Radecke**
  0000-0002-5815-5537 · julikaradecke
  Institute of Anatomy, University of Bern, Bern, Switzerland; Department of Neuroscience, Faculty of Health and Medical Science , 2200 Copenhagen N, University of Copenhagen, Copenhagen, Denmark; Diamond Light Source Ltd, Didcot, Oxfordshire, United Kingdom

- **Guillaume Witz**
  0000-0003-1562-4265 · guiwitz
  Science IT Service, University of Bern, Bern, Switzerland; Microscopy Imaging Center, University of Bern, Bern, Switzerland

- **Jakob B. Sørensen**
  0000-0001-5465-3769 · JBSorensen
  Department of Neuroscience, University of Copenhagen, Blegdamsvej 3B, 2200 Copenhagen N, Denmark · Funded by Novo Nordisk Fonden, NNF17OC0028516.; Carlsbergfondet, CF17-0875; Independent Research Fond Denmark, 8020-00228A; Lundbeckfonden, R277-2018-802

- **Benoît Zuber**✉
  0000-0001-7725-5579 · aseedb
  Institute of Anatomy, University of Bern, Bern, Switzerland · Funded by Swiss National Science Foundation, 179520; ERA-NET NEURON, NEURON-119

✉ Address correspondence to benoit.zuber@ana.unibe.ch.

* These authors contributed equally.

Abstract

Cryo-electron Tomography (Cryo-ET) has the potential to reveal cell structure down to atomic resolution. Nevertheless, cellular cryo-ET data is often highly complex and visualization, as well as quantification, of subcellular structures require image segmentation. Due to a relatively high level of noise and to anisotropic resolution in cryo-ET data, automatic segmentation based on classical computer vision approaches usually does not perform satisfyingly. For this reason, cryo-ET researchers have mostly performed manual segmentation.

Communication between neurons rely on neurotransmitter-filled synaptic vesicle (SV) exocytosis. Recruitment of SVs to the plasma membrane is an important means of regulating exocytosis and is influenced by interactions between SVs. Cryo-ET study of the spatial organization of SVs and of their interconnections allows a better understanding of the mechanisms of exocytosis regulation. To obtain a faithful representation of SV connectivity state, an absolutely vital prerequisite is an extremely accurate SV segmentation. Hundreds to thousands of SVs are present in a typical synapse, and their manual segmentation is a burden. Typically accurately segmenting all SVs in one synapse takes between 3 to 8 days. This segmentation process has been widely recognized as a bottleneck by the community.

Several attempts to automate vesicle segmentation by classical computer vision or machine learning algorithms have not yielded very robust results. We addressed this problem by designing a workflow consisting of a U-Net convolutional network followed by post-processing steps. This combination yields highly accurate results. Furthermore, we provide an interactive tool for accurately segmenting spherical vesicles in a fraction of the time required by available manual segmentation methods. This tool can be used to segment vesicles that were missed by the fully automatic procedure or to quickly segment a handful of vesicles, while bypassing the fully automatic procedure. Our pipeline can in principle be used to segment any spherical vesicle in any cell type as well as extracellular vesicles.

Introduction

The fine architecture of cells can be investigated by cryo-electron tomography (cryo-ET) [1]. Cellular structures are preserved down to the atomic scale through vitrification and observation of the samples in a fully hydrated state. When a macromolecule is present in a sufficient number of copies in the cells imaged by cryo-ET, it is possible to obtain its atomic structure in situ using subtomogram averaging [2,3]. Cellular cryo-ET datasets are usually extremely complex, making them difficult to analyze. This is aggravated by the sensitivity of biological samples to electron radiation, which limits the signal-to-noise ratio in cryo-ET datasets [4]. Tomographic reconstructions are generated from a series of images of the sample acquired at different viewing angles. The geometry of the samples prevents acquisition at certain angles, resulting in anisotropic spatial coverage. The resolution in the directions close to the axis of the electron beam incident on the untilted sample is strongly reduced. This effect, commonly referred to as the missing-wedge artifact, further complicates data analysis. In particular, organelles fully bounded by a membrane appear to have holes at their top and bottom (relative to the electron beam axis) [4].

The synapse is the functional cellular contact at which information is transmitted from a neuron to another. The former neuron is called presynaptic and the latter is postsynaptic. In most cases, the signal is transmitted by the release of neurotransmitters into the intercellular space. Neurotransmitters are stored in SVs and are released following the fusion of a vesicle with the presynaptic plasma membrane. A synapse contains hundreds of SVs and their mobility and recruitability for neurotransmitter release depends on inter-vesicle interactions through so-called connector structures [5]. The characterization of these interactions can be performed automatically

with the pyto software, which implements a hierarchical connectivity approach to detect and annotate connectors [6]. For accurate connector segmentation, an exceptionally precise segmentation of SVs is prerequisite. To date, this SV segmentation has been achieved manually, but given the massive number of SVs per dataset, it is an extremely time-consuming process. Typically, one person spends 3 to 8 working days to segment a single dataset. Attempts to perform this task automatically based on classical computer vision algorithms have not yielded sufficiently accurate performance [7].
To alleviate this situation, we considered applying deep learning methods.

Convolutional neural networks (CNN) have been successfully employed to segment cryo-ET data [8]. Although entirely satisfying for visualization purposes, this approach has not met the requirements of pyto. A recent publication described accurate SV segmentation of transmission electron microscopy images using CNN, but it is limited to 2-dimensional (2D) images of resin-embedded synapses [9]. In the first study, cryo-ET data are decomposed in individual 2D slices, which are handed as separate input to the CNN. The independent output 2D prediction images are reassembled in a 3-dimensional(3D) stack.[8] As discussed above, membranes oriented approximately parallel to the plane of the 2D tomographic images are not resolved. In the absence of contextual knowledge of the other 2D images, the CNN fails to segment these regions of the vesicles. Hence, spherical vesicles appear open, whereas we expect closed spherical objects. To overcome this limitation, we used a U-Net CNN that takes 3D images as input [10]. Weigert et al. [11] implemented a U-Net for content-aware restoration (CARE) of 3D fluorescence microscopy datasets. They showed that it can restore information from anisotropic and very noisy datasets. We implemented a 3D U-Net based on CARE building blocks and trained it with manually segmented datasets. This method provided good accuracy and was only slightly affected by the missing wedge artifact. Nevertheless, it was not sufficient for our downstream pyto analysis. Hence, we developed a post-processing method, which transforms the segmented objects into spheres and refines their radius and center location. The procedure includes an outlier detection procedure. This lead to a substantial accuracy improvement, which are reflected in better pyto performance. We also introduce a semi-automatic method to very quickly fix wrongly segmented or missed SVs.

Although our set of procedures was developed with the use case of SV segmentation in mind, it can be used to segment any other types of biological spherical vesicles, such as transport vesicles, secretory vesicles, endocytic vesicles, and extracellular vesicles.

Results

Cellular cryo-electron tomography is an upcoming field with a multitude of possible applications. The manual segmentation of the cellular features is a major bottleneck of this method. When segmenting cryo-electron tomograms from presynaptic terminals, the manual segmentation of synaptic vesicles is one of the most time-intensive steps. Synaptic vesicles constitute a large, homogeneous group, constituting a large training set for deep learning applications. Therefore, we decided to initially develop the automatic segmentation for synaptic vesicles. The used tomograms were previously manually segmented with IMOD, these manual segmentations were further treated as the ground truth [12]. `\_maybe add this somewhere else: In a next step, filaments connecting the synaptic vesicles with each other (connectors) and to the active zone (AZ) were automatically segmented with the algorithm application Pyto [@doi:10.1016/j.jsb.2016.10.004].*`

The U-Net neural network was used to train its mask prediction on a training set of 9 tomograms containing untreated synaptosomes. The learning progress was tracked by calculating the Dice coefficient and the loss value after each training epoch (Figure 1). The dice value for the training dataset started at a value of ~0.25 and rose to a value of over 0.9 after the initial 50 epoches. The loss value of the training dataset had an initial value of over 0.55 and declined to values below 0.05 after the initial 50 epochs and further striving towards 0 in the following depicted epochs. `\_Validation Dice and loss from treated synaptosome dataset?*` The validation dataset showed much more fluctuations during both validation and loss progression. The dice value for the validation dataset started at a value of ~0.27 and rose to an average value of over 0.75 after the initial 50 epoches. The loss value of the validation dataset had an initial value 1 and declined to values below 0.3 after the initial 50 epochs.

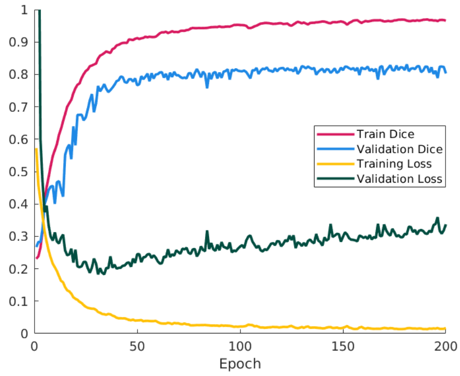

Figure 1: Dice coefficient and loss value for training and validation set. `\_legend in figure should say "Training Dice"*`

`\_---->add figures of local measurements such as diameter or center error as an extra figure, why else listed in M&M??"*`

After the neural network is trained to recognize the synaptic vesicles with a sufficient probability, the trained U-Net was implemented into a pipeline. The pipeline for automatic segmentation of vesicles consists of two major parts: the neural network consisting of a U-Net neural network, and the post-processing steps refining the labels generated by the U-Net (Figure 2). The three batches of tomograms (synaptosome control, synaptosome treatment and neuron) were each handed to the pipeline.

A B C D E

Tomogram 3D patches tomogram Segmentation Network Propability mask Stich patches back

F G H I J

Thresholding Adaptive localized Thresholding Outlier Removal Radial Profile Output

Figure 2: Pipeline of automatic segmentation. a) tomograms b) patchify the tomograms into 3D patches c) Segmentation Network/ trained U-Net d) probability masks e) stitching patches back together f) thresholding g) adaptive localized thresholding h) outlier removal i) radial profile

Each tomogram is split into patches of 32x32x32 `\_unit?*`. These patches are the fed into the trained U-Net, which outputs a probability mask for those patches. To obtain a complete probability mask, the patches are stitched back together. The probability mask is further refined by applying global and adaptive localized thresholding steps (Figure 2, Figure 3).

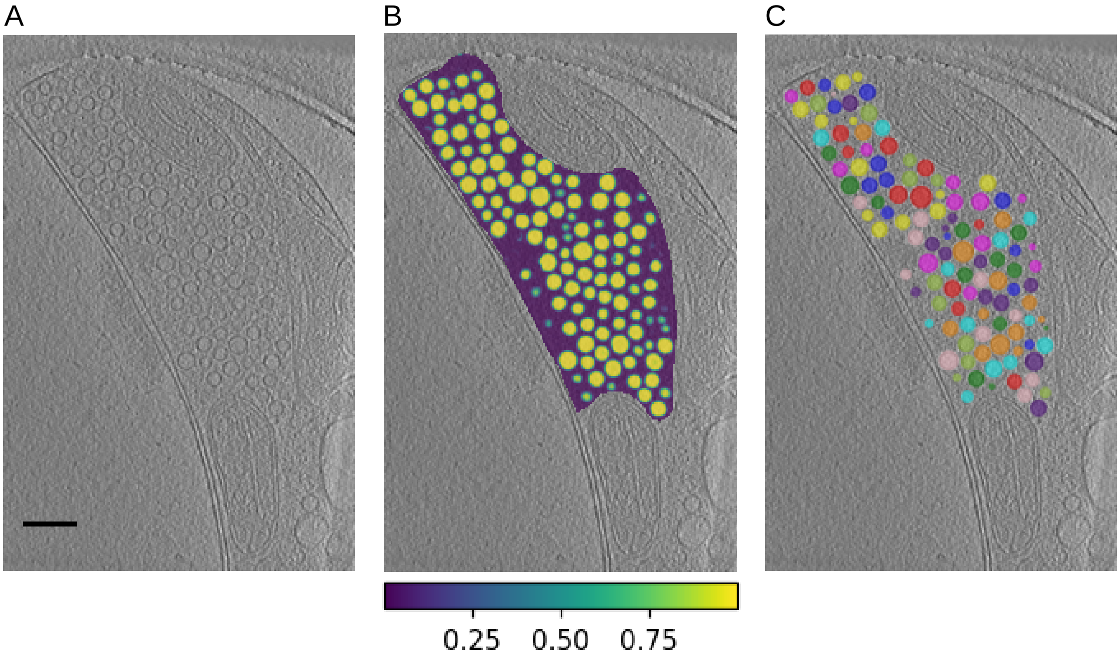

Figure 3: 2D Slices A) a section from z axis of a tomogram's presynaptic terminal of a neuron B) instance mask of the vesicles after post processing; purple corresponds to a low probability of SVs and yellow corresponds to a high probability of synaptic vesicles C) predicted probability mask by the segmentation network

_more detail about global and adaptive localized threshold* For further optimization of the mask, outliers were removed. Removed outliers mostly consisted of vesicles which were only partially segmented, and vesicles which maks were adjacent due to proximity. The removed masks, which only partially traced the vesicles, were reevaluated by reducing or expanding their radius (Figure 4). _was the center of the vesicles also reevaluated?* _Its not clear or might be false sentence we didnt remove or re evaluate the mask?*

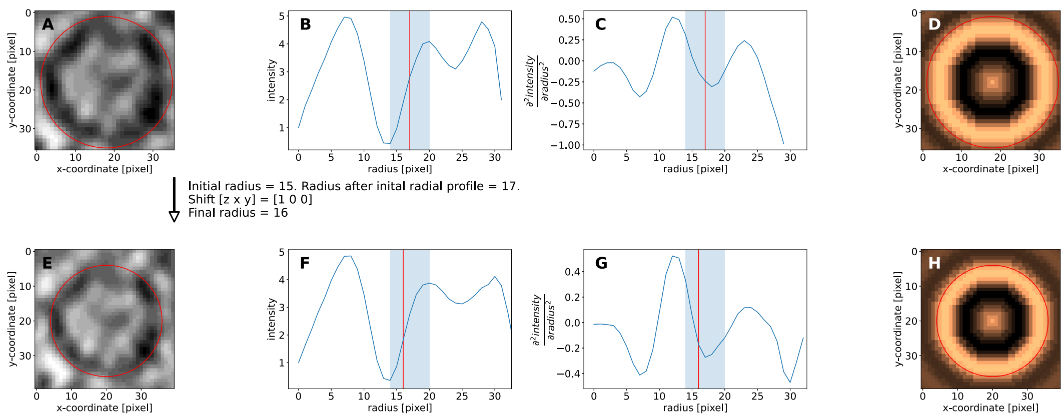

Figure 4: Vesicle radius and position through radial profile and cross-correlation Radial Profile Refinement A) couple of vesicles are not centered B) Radial Profile. Blue range is from membrane center to outer white halo center, this is the search range for the optimal radius. (smoothed by gaussian filtering) C) second derivative of radial profile E, F, H, G) Same as above columns after refinement

The adjacent vesicle masks were seperated (Figure _missing*). _how?*

_**missing Figure- Splitting adjacent vesicles. A) Examples of tomogram, no labels; B) raw label with connected vesicle-labels; C) modified label with seperated vesicles ---> for software: IMOD**

The Dice coefficient was used to track the global congruence between the manually segmented mask and the predicted mask within the different tomograms (Figure 5).

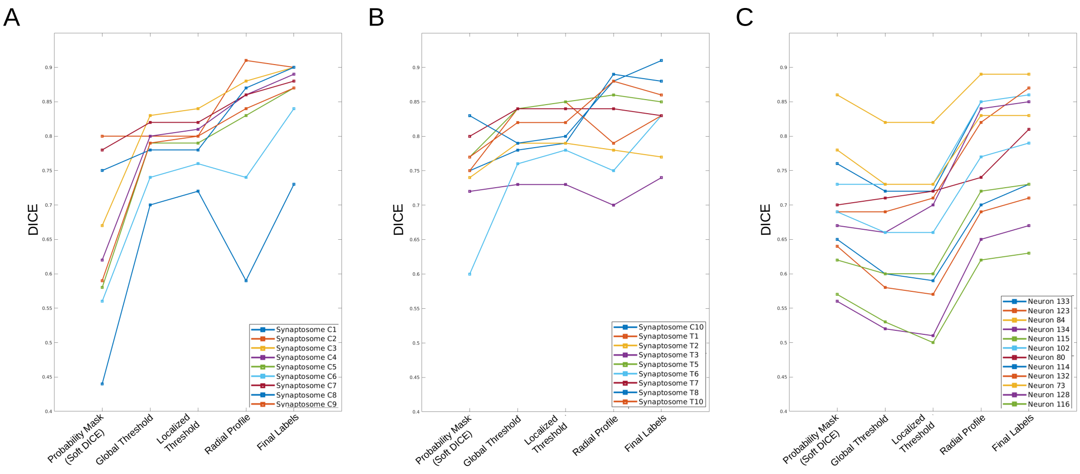

Figure 5: Dice developement during post-processing Dice developement at different post processing steps of initial predicted mask (different colors correspond to different tomograms): A) synaptosomal training datasets B) synaptosomal test datasets c) neuron test datasets

Final Eval Tables

Table 1- Evaluation of the segmentation: Mask Dice: Mask Dice coefficient for the predicted mask; Final Label Dice: Dice coefficient after post-processing; δ d: diameter error on correctly detected vesicle; Δ c: average error center (nm); # of Vesicles: number of expected vesicles; TP: True Positive; FN: False Negative; FP: False Positive

Train Dataset

Dataset	***Mask DICE***	***Final Label DICE***	***δ d***	***Δ c (nm)***	***# of Vesicles***	**TP**	**FN**	**FP**
Synaptosome C1	0.44	0.73	0.07	2.55±1.56	223	198	26	49
Synaptosome C2	0.8	0.9	0.05	2.12±1.06	105	103	2	1
Synaptosome C3	0.67	0.9	0.05	1.86±1.24	128	127	1	6
Synaptosome C4	0.62	0.89	0.03	1.78±0.92	144	141	3	4
Synaptosome C5	0.58	0.87	0.04	1.86±1.00	214	209	5	13
Synaptosome C6	0.56	0.84	0.04	1.92±1.05	104	102	2	16
Synaptosome C7	0.78	0.88	0.06	1.86±0.90	184	184	0	16
Synaptosome C8	0.75	0.9	0.05	1.70±0.93	132	126	6	1
Synaptosome C9	0.59	0.87	0.05	1.87±0.91	135	132	3	14
Average	**0.64±0.11**	**0.86±0.05**	**0.05**	**1.95±1.08**	**152.22**	**97.00%**	**3.00%**	**7.30%**

Test Dataset (Same preparation and microscope with training set)

Dataset	***Mask DICE***	***Final Label DICE***	***δ d***	***Δ c (nm)***	***# of Vesicles***	**TP**	**FN**	**FP**
Synaptosome C10	0.75	0.88	0.07	1.86±1.18	129	123	6	5
Synaptosome T1	0.75	0.83	0.11	2.66±1.52	699	687	12	33
Synaptosome T2	0.74	0.77	0.11	2.27±1.84	122	117	5	2
Synaptosome T3	0.72	0.74	0.11	3.64±2.22	434	397	37	57

Dataset	*Mask DICE*	*Final Label DICE*		*δ d*	*Δ c (nm)*	*# of Vesicles*	**TP**	**FN**	**FP**
Synaptosome T5	0.77	0.85		0.08	2.20±1.26	535	526	9	25
Synaptosome T6	0.6	0.83		0.07	2.02±1.12	373	353	20	42
Synaptosome T7	0.8	0.83		0.06	2.22±1.14	110	107	3	9
Synaptosome T8	0.83	0.91		0.04	2.09±1.04	100	99	1	2
Synaptosome T10	0.77	0.86		0.05	1.96±1.04	77	74	3	6
Average	**0.75±0.06**	**0.83±0.05**		**0.08**	**2.32±1.43**	**286.56**	**96.30%**	**3.70%**	**6.10%**

Test Dataset 3 (Neuron Dataset)

Dataset	*Mask DICE*	*Final Label DICE*		*δ d*	*Δ c (nm)*	*# of Vesicles*	**TP**	**FN**	**FP**
Neuron 133	0.76	0.86		0.05	2.16±1.32	523	467	56	8
Neuron 123	0.64	0.71		0.05	2.05±1.18	66	58	8	2
Neuron 84	0.86	0.89		0.06	1.44±0.75	498	484	14	1
Neuron 134	0.56	0.67		0.09	2.87±2.50	638	384	254	63
Neuron 115	0.57	0.63		0.08	3.56±3.23	170	123	47	32
Neuron 102	0.73	0.86		0.05	1.47±0.79	103	86	17	1
Neuron 80	0.7	0.81		0.07	2.67±2.00	111	102	9	3
Neuron 114	0.65	0.73		0.07	2.68±1.79	131	93	38	9
Neuron 132	0.69	0.87		0.03	1.65±1.26	135	129	6	32
Neuron 73	0.78	0.83		0.06	2.93±2.00	526	483	43	2
Neuron 128	0.67	0.85		0.04	2.33±1.70	252	232	20	19
Neuron 116	0.62	0.73		0.07	2.38±1.82	296	207	89	35
Average	**0.69±0.09**	**0.79±0.09**		**0.06**	**2.35±1.83**	**287.42**	**83.60%**	**16.40%**	**7.90%**

Our method transfers well across datasets even without fine-tuning which show robustness and generalization.

Comparison of manual segmentation with automatic deep-learning based segmentation

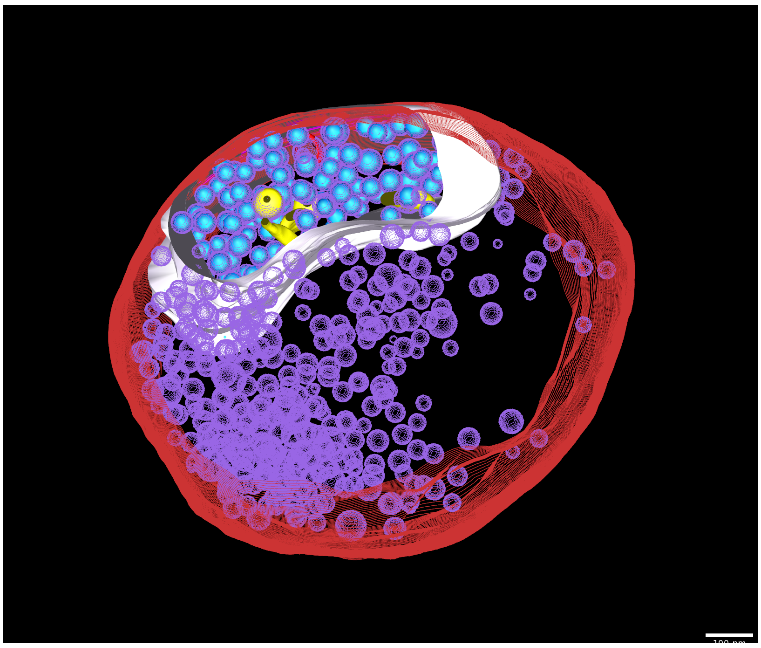

Figure 6: 3D model of manual segmented and automatically segmented synaptosome.

Discussion

While the Dice coefficient is a good global measure to assess the predictions in comparison to the ground truth, it is difficult to asses local segmentation accurracy. For example, a single generated vesicle label containing several close connected vesicles would not be practical for further analysis for the researcher although it could have almost the same dice value. What is important for actual usage of the software would be the number and percentage of true-detected vesicles, false-positive and false-negative rates.

Center error: If we measure each axis error it will reveal that human bias in segmentation is more affected on the Z-axis. [we didn't show it in number but its checked the hypothesis] `\_we cannot claim something without showing it. ---> this would belong into results*`

3d unet good for 3D processing recent Nature methods paper by Ben Engel, DeepFinder -> Relion for STA creates mask to find more using dl -what are they doing, maybe compare that in the text, different aims; we might compare results we achieve (keep as bonus, revision)

Outlook

implement automatic cell-outline and active zone segmentation as deep learning workflow using UNet implement automatic connector and tether segmentation as a deep leaning workflow using UNet

Materials and methods

Cryo-electron Tomography Datasets

Two datasets of different origin were used as input and test subjects for the automatic segmentation pipeline, respectively. They consisted in rat synaptosomes primary neuron cultures derived from mice. The preparation procedure of the samples from which the datasets were obtained as well as the biological analysis of these datasets was previously reported [13].

Manual segmentation and automatic interboundary segment detection

Manual segmentation of SVs, mitochondria, the active zone PM, and of the segmentation region was done in IMOD (???Figure S4A&B???) [12]. SVs were segmented as spheres. The segmentation region marked the region to be analyzed by Pyto [6]. The analysis by Pyto was essentially the same as described previously [5,6]. In short, the segmented region is divided in 1 voxel thick layers parallel to the active zone for distance calculations. A hierarchical connectivity segmentation detects densities interconnecting boundaries. The boundaries were synaptic vesicles and the active zone PM. Detected intervesicular segments are termed connectors and segments connecting vesicles to the active zone PM are called tethers (Figure `\_add figure number*`). Distance calculations respective to SVs were done from SV center. The segmentation procedure is conservative and tends to miss some tethers and connectors because of noise. Consequently, the numbers of tethers and connectors should not be considered as absolute values, but rather to compare experimental groups. As it was done before, an upper limit was set between 2100 and 3200 nm^3 on segment volume. The tomograms that were used for this analysis were binned by a factor of 2 to 3, resulting in voxel sizes between 2.1 and 2.4 nm.

Pre-processing of manual segmentation outputs from IMOD for further use (jupyter notebook pre-pyto)

`probably not necessary to mention output from IMOD to prepyto input label file procedure`

`put this somewhere else`.{green} The used datasets included a total of 30 tomograms with heterogeneous pixel sizes, defocus and resolution.

1. 9 synaptosome datasets were used for training and validation.
2. 9 synaptosome datasets was used for test.
3. 12 Neuron dataset were used for assessing transfer learning potential.

Network architecture and training procedure

We used a U-Net of depth 2, two convolutional layers per depth, a convolutional kernel size of 3, and ReLU activation function based on the open-source CARE framework (Figure 7) [11]. Datasets were prepared by splitting the 3D tomographic volume of synaptosomes into 32^3 voxels subvolumes and keeping only subvolumes occupied by a sufficient amount (> 1000 voxels) of binarized vesicle label. 860 subvolumes were used for training and 100 subvolumes were used for validation. We used the Adam optimizer on a binary cross-entropy loss function.

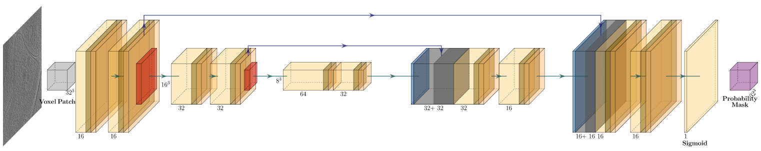

Figure 7: Network architecture used for vesicle segmentation. We used a U-Net based on the CARE framework [11]. The input is a cubic volume of 32^3 voxels. The output is a per-prix probabilty cube of the same size as the input.

U-Net output threshold refinement

The probability mask output by the U-Net was first made binary by determining a global threshold value. To this end, the mask was binarized for a range of threshold values comprised between 0.8 and

1. For each probability value a 1-voxel thick label shell was computed. The shell mask was then applied on the input data and the average masked voxel intensity was computed. Since the shell of correctly segmented vesicles corresponds to the vesicle membrane, we expect low intensity pixels. The threshold value resulting in the minimal average intensity of the shell masked voxels was used as the global threshold.
`Amin please write the equations for these steps`.{green}. The probability mask was binarized using the global threshold and was each separate segment was assigned an individual label with `scikit-image label` method.

A majority of vesicles were correctly segmented but we noticed some segments included two vesicles. We therefore evaluated each segment with two criteria based on the fact that synaptic vesicles have a homogenous size and are spherical. Firstly we calculated the volume z-score z for each segment:

$$z(i) = \frac{v(i) - \mu(v)}{\sigma(v)} \tag{1}$$

where $v(i)$ is the volume of segment i, (v) the average segment volume, and $\sigma(v)$ the standard deviation of the segment volumes. Secondly, we computed the segment extent e:

$$e(i) = \frac{v(i)}{b(i)} \tag{2}$$

where $v(i)$ is the segment volume and b_i is the volume of segment bounding box. The extent of a sphere equals $\frac{\pi}{6}$. Segments with both a z-score $z > 1$ and an extent $e < 0.25$ were considered as potentially comprising two vesicles. For each of these segments, the probability mask threshold was increased until two distinct segments were generated.

Radial Profile

`\_@Benoit?*`

Outlier Removal

The feature space of predicted vesicle labels was defined, containing thickness, membrane density, and estimated radius of a vesicle. `\_@Benoit: after radial profile, we can add the definition of thinness and membrane as well*` To detect outliers in this multivariate space, Mahalanobis Distance (MD) was applied to calculate L2 norm distance on normalized variables using the covariance matrix of observation. As an additional way to detect outliers, the p-value of MD was calculated, bringing this evaluation setup in iterative form. If the MD p-value of a specific vesicle was not in a specific margin range (0-10), their radial profile was recalculated, and the label entirely removed if they again failed to pass the margin of the p-value.

Radius Estimation (Cross Correlation through Radial Profile)

`\_@Benoit?*`

Analysis of Results

The evaluation framework was designed to assess the capabilities of the proposed toolbox for automatic synaptic vesicle segmentation. The framework was not only designed to evaluate quantitatively performance of the neural network, but rather assay the segmentation of vesicles in practice `\_unsure what the last part means*`. `\_I tried to say we develop the` software rather than an algorithm paper with ablation study kinda more trasnfer learning but however for tranfer learning we might need add finetunning the network or say this sentence in other way*. The pipeline also generates a specific output format, which is necessary to further analyze the presynaptic tomograms via another pre-developed toolbox (Pyto), which segments small molecular filaments associated to the synaptic vesicles, titled tethers and connectors.

DICE

The _general form??* DICE coefficient for probabilistic subvolume maps was calculated after each epoch as a performance quantification while _during?* training. The probabilistic mask subvolumes were stitched back together, creating a probabilistic map of the whole tomogram. The Soft-DICE for the whole tomogram was calculated to evaluate the similarity of the predicted probability mask with ground truth. Note that soft-dice is equivalent to dice, when the input is binarized (which we will do at the end of the post-processing).

$$1 - \frac{2\sum_{pixels} y_{true}y_{pred}}{\sum_{pixels} y_{true}^2 + \sum_{pixels} y_{pred}^2}$$

_shouln't it be voxels instead of pixels??* _yes voxel is right*

THE DICE was also employed to monitor all stages of post-processing on the eventual label file, to observe the effect of each post-processing step.

Diameter Error

The diameter of a vesicle is one of its relevant characterizations, and it is predefined (see Outlier Removal). _which diameters are we using in this evaluation as input, pre- or post-outlier removal?* _after! I meant from that perentesis that radius or dimater we assume as one charectiristic of vesicle we might can write it better * The error of diameter estimation of true-detected vesicle is defined as 1 minus the proportion of diameters

$$\delta d = 1 - \frac{min(dSi, dGTi)}{max(dSi, dGTi)} \tag{3}$$

where dGTi is the diameter of each true manual segmented vesicle, and dSi is the diameter of its estimation.

Center error

The center error is an euclidean distance of ground truth and corresponds to true predicted vesicles _true pos or true neg*. A vesicle was defined as a true-detected vesicle if the predicted center was located inside the hand-segmented vesicle and the other way around the center of prediction was located inside the predicted vesicle. _isn't this a bit too general, shouldn't this be a tighter evaluation?* _we assume this as hard condition to be true postive we could define like some % liek 50% intersection but this condition is generally harder This means the volume of intersection of the estimated vesicle with the distance of d to a ground truth vesicle with radius R is:

$$V = \frac{1}{12}\pi(4R + d)(2R - d)$$

Manuscript preparation

The manuscript was written with the open and collaborative scientific writing package Manubot [14]. The source code and data for this manuscript are available at https://github.com/aseedb/synaptic_tomo_ms.

References

1. **Towards Visual Proteomics at High Resolution**
Felix JB Bäuerlein, Wolfgang Baumeister
Journal of Molecular Biology (2021-10) https://doi.org/gn9t3v
DOI: 10.1016/j.jmb.2021.167187 · PMID: 34384780

2. **Exploring high-resolution cryo-ET and subtomogram averaging capabilities of contemporary DEDs**
Martin Obr, Wim JH Hagen, Robert A Dick, Lingbo Yu, Abhay Kotecha, Florian KM Schur
Cold Spring Harbor Laboratory (2022-01-10) https://doi.org/gn92pd
DOI: 10.1101/2022.01.10.475481

3. **High-resolution in situ structure determination by cryo-electron tomography and subtomogram averaging using emClarity**
Tao Ni, Thomas Frosio, Luiza Mendonça, Yuewen Sheng, Daniel Clare, Benjamin A Himes, Peijun Zhang
Nature Protocols (2022-01-12) https://doi.org/gn92pc
DOI: 10.1038/s41596-021-00648-5 · PMID: 35022621 · PMCID: PMC9251519

4. **STRUCTURAL STUDIES BY ELECTRON TOMOGRAPHY: From Cells to Molecules**
Vladan Lučić, Friedrich Förster, Wolfgang Baumeister
Annual Review of Biochemistry (2005-06-01) https://doi.org/cfd27f
DOI: 10.1146/annurev.biochem.73.011303.074112 · PMID: 15952904

5. **Quantitative analysis of the native presynaptic cytomatrix by cryoelectron tomography**
Rubén Fernández-Busnadiego, Benoît Zuber, Ulrike Elisabeth Maurer, Marek Cyrklaff, Wolfgang Baumeister, Vladan Lučić
Journal of Cell Biology (2010-01-11) https://doi.org/b9c26b
DOI: 10.1083/jcb.200908082 · PMID: 20065095 · PMCID: PMC2812849

6. **Hierarchical detection and analysis of macromolecular complexes in cryo-electron tomograms using Pyto software**
Vladan Lučić, Rubén Fernández-Busnadiego, Ulrike Laugks, Wolfgang Baumeister
Journal of Structural Biology (2016-12) https://doi.org/f9d5t2
DOI: 10.1016/j.jsb.2016.10.004 · PMID: 27742578

7. **Robust membrane detection based on tensor voting for electron tomography**
Antonio Martinez-Sanchez, Inmaculada Garcia, Shoh Asano, Vladan Lucic, Jose-Jesus Fernandez
Journal of Structural Biology (2014-04) https://doi.org/f5zkj8
DOI: 10.1016/j.jsb.2014.02.015 · PMID: 24625523

8. **Convolutional neural networks for automated annotation of cellular cryo-electron tomograms**
Muyuan Chen, Wei Dai, Stella Y Sun, Darius Jonasch, Cynthia Y He, Michael F Schmid, Wah Chiu, Steven J Ludtke
Nature Methods (2017-08-28) https://doi.org/gkpj62
DOI: 10.1038/nmeth.4405 · PMID: 28846087 · PMCID: PMC5623144

9. **Automated Detection and Localization of Synaptic Vesicles in Electron Microscopy Images**
Barbara Imbrosci, Dietmar Schmitz, Marta Orlando
eneuro (2022-01) https://doi.org/gn9n8k
DOI: 10.1523/eneuro.0400-20.2021 · PMID: 34983830 · PMCID: PMC8805189

10. **3D U-Net: Learning Dense Volumetric Segmentation from Sparse Annotation**
Özgün Çiçek, Ahmed Abdulkadir, Soeren S Lienkamp, Thomas Brox, Olaf Ronneberger
arXiv (2016-06-22) https://arxiv.org/abs/1606.06650

11. **Content-aware image restoration: pushing the limits of fluorescence microscopy**
Martin Weigert, Uwe Schmidt, Tobias Boothe, Andreas Müller, Alexandr Dibrov, Akanksha Jain, Benjamin Wilhelm, Deborah Schmidt, Coleman Broaddus, Siân Culley, … Eugene W Myers
Nature Methods (2018-11-26) https://doi.org/gfkkfd
DOI: 10.1038/s41592-018-0216-7 · PMID: 30478326

12. **Computer Visualization of Three-Dimensional Image Data Using IMOD**
James R Kremer, David N Mastronarde, JRichard McIntosh
Journal of Structural Biology (1996-01) https://doi.org/d9nfzw
DOI: 10.1006/jsbi.1996.0013 · PMID: 8742726

13. **Morphofunctional changes at the active zone during synaptic vesicle exocytosis**
Julika Radecke, Raphaela Seeger, Anna Kádková, Ulrike Laugks, Amin Khosrozadeh, Kenneth N Goldie, Vladan Lučić, Jakob B Sørensen, Benoît Zuber
Cold Spring Harbor Laboratory (2022-03-07) https://doi.org/gpm26v
DOI: 10.1101/2022.03.07.483217

14. **Open collaborative writing with Manubot**
Daniel S Himmelstein, Vincent Rubinetti, David R Slochower, Dongbo Hu, Venkat S Malladi, Casey S Greene, Anthony Gitter
PLOS Computational Biology (2019-06-24) https://doi.org/c7np
DOI: 10.1371/journal.pcbi.1007128 · PMID: 31233491 · PMCID: PMC6611653